



Amplitude analysis of the $B^0 \rightarrow K^{*0} \mu^+ \mu^-$ decay

LHCb collaboration[†]

Abstract

An amplitude analysis of the $B^0 \rightarrow K^{*0} \mu^+ \mu^-$ decay is presented using a dataset corresponding to an integrated luminosity of 4.7 fb^{-1} of pp collision data collected with the LHCb experiment. For the first time, the coefficients associated to short-distance physics effects, sensitive to processes beyond the Standard Model, are extracted directly from the data through a q^2 -unbinned amplitude analysis, where q^2 is the $\mu^+ \mu^-$ invariant mass squared. Long-distance contributions, which originate from non-factorisable QCD processes, are systematically investigated and the most accurate assessment to date of their impact on the physical observables is obtained. The pattern of measured corrections to the short-distance couplings is found to be consistent with previous analyses of b - to s -quark transitions, with the largest discrepancy from the Standard Model predictions found to be at the level of 1.8 standard deviations. The global significance of the observed differences in the decay is 1.4 standard deviations.

Published in Phys. Rev. Lett. 132 (2024) 131801

© 2024 CERN for the benefit of the LHCb collaboration. CC BY 4.0 licence.

[†]Authors are listed at the end of this Letter.

Flavour-changing neutral current (FCNC) processes involving the transition of a beauty into a strange quark provide powerful indirect probes for effects beyond the Standard Model (SM). These transitions are mediated through virtual quantum loops in the SM, and as yet undiscovered particles may contribute to the transition amplitudes of the decay at a level comparable to SM processes. These new contributions can cause deviations in the decay rate or in the angular distributions of the final-state particles. Past studies of these processes have shown an intriguing set of discrepancies with respect to the SM predictions [1–5]. In particular, analyses of the $B^0 \rightarrow K^{*0} \mu^+ \mu^-$ decay have reported statistically significant deviations in the branching fraction [6] and in the angular distributions of the decay [7–13], notably in observables with reduced theoretical uncertainties, *e.g.* in the so-called P'_5 observable [14].

Beauty- to strange-quark FCNC processes are typically described within an effective field theory [15] in terms of four-fermion interactions. Within this framework, the strengths of the different types of interaction are encoded by the so-called Wilson coefficients, labelled as $\mathcal{C}_i^{(\prime)}$, and beyond the Standard Model (BSM) effects would appear as a deviation in the values of one or more Wilson coefficients. The most relevant contributions are from the so-called electromagnetic dipole operator and from vector and axial-vector interactions as shown in Fig. 1, with coefficients \mathcal{C}_7 , \mathcal{C}_9 and \mathcal{C}_{10} , respectively, and their counterparts with the opposite chirality, \mathcal{C}'_i , which are suppressed in the SM. Global analyses of $b \rightarrow s$ transitions have reported deviations from the SM expectations with significances as large as 4 standard deviations [16–19]. The largest tensions are seen in the real part of \mathcal{C}_9 . The interpretation of the global analyses is complicated by large theoretical uncertainties on the prediction of non-factorisable (long-distance) hadronic contributions that can mimic BSM effects [20, 21]. In order to improve the sensitivity of the global analyses, it is imperative to find reliable ways of reducing the impact of these uncertainties. Since the first measurement of P'_5 by LHCb in 2013 [8], progress has been made on the uncertainties of SM predictions [22–37], and the most recent developments suggest that it is now possible to control the size of the long-distance contributions in data [16]. Nevertheless, no definitive consensus on the characterisation of these effects has been reached yet [19].

This Letter reports the first unbinned amplitude analysis of the decay $B^0 \rightarrow K^{*0} \mu^+ \mu^-$ that determines simultaneously the short- and long-distance contributions.¹ The strategy of this analysis is based on the methodology discussed in Refs. [16, 37–39], and allows a systematic evaluation of the impact of theoretical uncertainties on the observables of interest. A more comprehensive description of these studies is reported in a companion article [40].

The differential decay rate for the $B^0 \rightarrow K^{*0} \mu^+ \mu^-$ decay, where the K^{*0} meson is reconstructed through the decay $K^{*0} \rightarrow K^+ \pi^-$, is fully described by five kinematic variables: the invariant mass squared of the $\mu^+ \mu^-$ system, q^2 , the invariant mass squared of the $K^+ \pi^-$ system, k^2 , and the three angles $\vec{\Omega} = (\cos \theta_\ell, \cos \theta_K, \phi)$ [41]. The angular basis used in this work is defined in Ref. [7]. The five-dimensional differential decay rate

¹Throughout this Letter, K^{*0} is used to refer to the $K^*(892)^0$ resonance and the inclusion of charge-conjugate processes is implied.

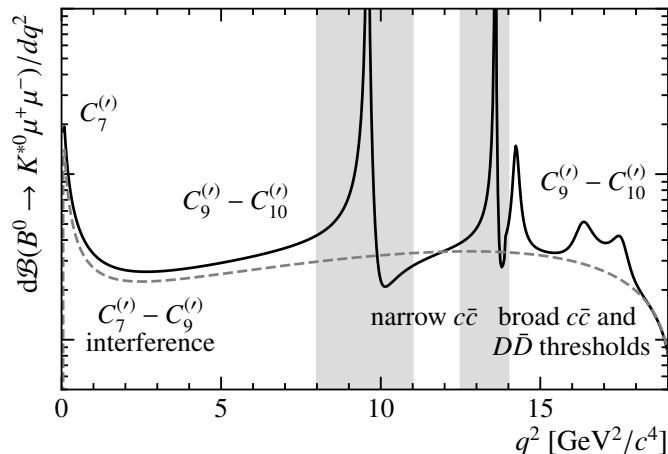


Figure 1: Illustration of the q^2 spectrum in $B^0 \rightarrow K^{*0} \mu^+ \mu^-$ decays. The dashed line corresponds to the pure rare semileptonic decay, while the solid line includes the impact of different charmonium resonances. The gray bands correspond to the regions dominated by $B^0 \rightarrow J/\psi K^{*0}$ and $B^0 \rightarrow \psi(2S) K^{*0}$ tree-level decays. Magnitudes and phases of $c\bar{c}$ resonant components have been arbitrarily chosen for illustrative purposes. The dominant Wilson coefficients in each region of the spectrum are also highlighted for reference.

$d^5\Gamma/(dq^2 dk^2 d\vec{\Omega})$ can be computed from combinations of decay amplitudes [26, 37, 42]

$$\mathcal{A}_\lambda^{L,R} = \mathcal{N} \left\{ \left[(\mathcal{C}_9 \pm \mathcal{C}'_9) \mp (\mathcal{C}_{10} \pm \mathcal{C}'_{10}) \right] \mathcal{F}_\lambda(q^2, k^2) + \frac{2m_b M_B}{q^2} \left[(\mathcal{C}_7 \pm \mathcal{C}'_7) \mathcal{F}_\lambda^T(q^2, k^2) - 16\pi^2 \frac{M_B}{m_b} \mathcal{H}_\lambda(q^2, k^2) \right] \right\} \quad (1)$$

and corresponding angular terms [41, 42], where $\lambda = 0, \parallel, \perp$ refers to the polarisation of the K^{*0} meson, L and R to the left- and right-hand chirality of the dimuon current, \mathcal{N} is a normalization factor and m_b and M_B are the masses of the b quark and the B meson [43]. Finally, all non-perturbative effects are contained within the local, $\mathcal{F}_\lambda^{(T)}$, and non-local, \mathcal{H}_λ , form-factors (FFs). The numerical values for the Wilson coefficients at the b -quark mass scale of $\mu_b = 4.2 \text{ GeV}/c^2$ are calculated in the SM as $\mathcal{C}_7^{\text{SM}} = -0.337$, $\mathcal{C}_9^{\text{SM}} = 4.27$, $\mathcal{C}_{10}^{\text{SM}} = -4.17$, and $\mathcal{C}'_{7,9,10}^{\text{SM}} \simeq 0$ [44, 45]. Local form-factors can be assessed by light-cone sum rules [22–26] and lattice QCD [27–31] techniques. Non-local contributions from $b \rightarrow c\bar{c}s$ operators are more difficult to calculate reliably from first principles and only recently a rigorous approach that relies on the analytical structure of these matrix elements has been formulated [16, 37]. This approach isolates the ψ_n resonance poles, where ψ_n is a J/ψ or $\psi(2S)$ state, and constructs a polynomial expansion for the remaining contributions in terms of a conformal variable, $z(q^2)$. In order to acquire control over the size of the coefficients of the expansion, data on $B^0 \rightarrow \psi_n K^{*0}$ decays as well as SM predictions [36] for the ratios $\mathcal{H}_\lambda/\mathcal{F}_\lambda$ at negative q^2 are employed. In this Letter, the role of the theoretical inputs on the determination of non-local effects (\mathcal{H}_λ) is examined, as well as their impact on the estimation of short-distance physics parameters ($\mathcal{C}_i^{(\prime)}$ and \mathcal{F}_λ).

The observed $B^0 \rightarrow K^+ \pi^- \mu^+ \mu^-$ differential decay rate receives a non-negligible contribution from decays where the $K^+ \pi^-$ system appears in a scalar (S-wave) configuration [6].

This is taken into account by introducing an additional pair of decay amplitudes and allowing interference and pure S-wave angular terms in the differential decay rate [46, 47]. Non-local contributions to the S-wave amplitudes are neglected, while their normalisation is decoupled from the $B^0 \rightarrow K^{*0} \mu^+ \mu^-$ amplitudes by introducing a complex coefficient that describes the relative magnitude and phases to be determined from data. Finally, the absolute scale of the Wilson coefficients is set by the branching fraction of the decay, which is related to the integral of the differential decay rate over the desired q^2 and k^2 ranges through

$$\mathcal{B}(B^0 \rightarrow K^{*0} \mu^+ \mu^-) = \frac{\tau_B}{\hbar} \int_{q_{\min}^2}^{q_{\max}^2} \int_{k_{\min}^2}^{k_{\max}^2} \frac{d^2\Gamma}{dq^2 dk^2} dq^2 dk^2, \quad (2)$$

where τ_B is the lifetime of the B^0 meson.

The dataset used in this analysis is the same as employed in Ref. [10] and corresponds to an integrated luminosity of 4.7 fb^{-1} of proton-proton (pp) collisions collected with the LHCb experiment during 2011, 2012 and 2016. The LHCb detector is a single-arm forward spectrometer covering the pseudorapidity range $2 < \eta < 5$, described in detail in Refs. [48, 49]. Samples of simulated events produced with the software described in Refs. [50–53] are used to determine the reconstruction and selection efficiencies for signal candidates and to estimate the contamination from residual backgrounds. Inaccuracies in the simulations are corrected for using control samples from data.

The K^{*0} candidates are selected with $K^+ \pi^-$ invariant mass within $100 \text{ MeV}/c^2$ of the known K^{*0} mass [43]. Candidates with $q^2 < 1.1$ or $q^2 > 15.0 \text{ GeV}^2/c^4$ are excluded, to remove contributions from light-quark resonances and from charmonium states beyond the open-charm threshold, respectively. Signal candidates are selected in two q^2 regions, $[1.1, 8.0]$ and $[11.0, 12.5] \text{ GeV}^2/c^4$, while the tree-level decays $B^0 \rightarrow J/\psi K^{*0}$ and $B^0 \rightarrow \psi(2S) K^{*0}$, where the charmonium resonance decays to $\mu^+ \mu^-$, are retained as control regions in the intervals $[8.0, 11.0]$ and $[12.5, 15.0] \text{ GeV}^2/c^4$, respectively, in order to validate several procedures of the analysis. A total of 2568 ± 60 signal decays and approximately 677 000 $B^0 \rightarrow J/\psi K^{*0}$ and 43 700 $B^0 \rightarrow \psi(2S) K^{*0}$ decays are selected.

The variation of the efficiency to reconstruct and select the signal across the kinematic phase space is accounted for in the fit by multiplying the differential decay rate by an efficiency function obtained from simulated samples. This efficiency function is parameterised using different orders of Legendre polynomials, each depending on one angle or q^2 , without assuming factorisation. No significant dependence of the efficiency on k^2 is observed. Moreover, the relative efficiency between rare and control modes is obtained from these simulations and the efficiency model is validated by comparing the measured ratio of branching fractions of the two control modes to its known value [43].

An extended unbinned maximum-likelihood fit to the five-dimensional differential decay rate, in q^2 , k^2 and the three decay angles, and the B -candidate invariant mass distribution, $m_{K\pi\mu\mu}$, is performed using the TENSORFLOW library [54] with an interface to the MINUIT minimisation algorithm [55, 56]. The $m_{K\pi\mu\mu}$ distribution is used in the fit to discriminate signal from background, where the background is composed primarily from random combination of tracks. The real parts of the $\mathcal{C}_9^{(\prime)}$ and $\mathcal{C}_{10}^{(\prime)}$ coefficients are allowed to vary in the fit, while the coefficients $\mathcal{C}_7^{(\prime)}$, which are strongly constrained by radiative B decays [57], are fixed to their SM values. Since B^0 and \bar{B}^0 decays are treated jointly in the analysis, only the CP -averaged decay rate is accessed and no sensitivity to the imaginary

part of the Wilson coefficients can be achieved. In addition to the above-mentioned Wilson coefficients, a large number of signal parameters is extracted simultaneously from the fit to data: the local and non-local FF parameters, the Cabibbo-Kobayashi-Maskawa (CKM) factor $V_{tb}V_{ts}^*$ that enters in the normalisation of Eq. 1 and the S-wave relative magnitude and phase, while the local S-wave FFs are treated as nuisance parameters.

The convergence of the polynomial expansion employed to model the non-local hadronic contributions \mathcal{H}_λ is carefully investigated. The polynomial expansion is performed around $q^2 = 0$, the truncation point of the expansion is chosen by repeating the fit with increasing orders of polynomials and the Akaike information criterion [58] is used to decide on the statistical relevance of each additional set of coefficients. A fourth-order expansion is found to be sufficient. The B -candidate mass distribution for the signal is parameterised by a sum of two Crystal Ball functions [59]. Finally, the k^2 dependence of the signal amplitudes is modelled using a relativistic Breit–Wigner function for the spin-1 K^{*0} resonance and the LASS parameterisation [60] for the S-wave component.

The background is modelled by second-order polynomial functions of the decay angles and q^2 , whose coefficients are allowed to vary in the fit. The k^2 distribution is described by the sum of a linear function and a Breit–Wigner amplitude squared, where the former accounts for a pure combinatorial component and the latter accommodates genuine K^{*0} resonances associated with random μ^+ and μ^- tracks. The reconstructed B mass distribution of the background is parameterised by an exponential function. A significant sculpting of $\cos\theta_K$ as a function of q^2 and $m_{K\pi\mu\mu}$ is observed due to a kinematic veto used to reject $B^+ \rightarrow K^+\mu^+\mu^-$ decays. This distortion is accounted for by multiplying the combinatorial background parameterisation by a three-dimensional efficiency correction factor obtained from a $B^0 \rightarrow K^{*0}e^\pm\mu^\mp$ control sample.

The observed signal yield determined by the extended fit is expressed in terms of the branching fraction of the decay given in Eq. 2 through

$$N_{\text{sig}} = N_{J/\psi K\pi} \times \frac{\mathcal{B}(B^0 \rightarrow K^{*0}\mu^+\mu^-) \times \frac{2}{3}}{\mathcal{B}(B^0 \rightarrow J/\psi K^+\pi^-) \times f^{J/\psi K\pi} \times \mathcal{B}(J/\psi \rightarrow \mu^+\mu^-)} \times R_\varepsilon, \quad (3)$$

where the factor $\frac{2}{3}$ comes from the $K^{*0} \rightarrow K^+\pi^-$ decay probability and the signal branching fraction is normalised to the $B^0 \rightarrow J/\psi K^+\pi^-$ control channel in order to reduce the associated systematic uncertainty. The yield of the control channel, $N_{J/\psi K\pi}$, is obtained directly from a mass fit, while the resonant and charmonium branching ratios $\mathcal{B}(B^0 \rightarrow J/\psi K^+\pi^-) = (1.15 \pm 0.01 \pm 0.05) \times 10^{-3}$ and $\mathcal{B}(J/\psi \rightarrow \mu^+\mu^-) = (5.96 \pm 0.03) \times 10^{-2}$ are taken from Refs. [61] and [43], respectively. The numerical factor $f^{J/\psi K\pi} = 0.644 \pm 0.010$ scales the total $B \rightarrow J/\psi K^+\pi^-$ branching ratio in the k^2 range of this analysis [40] and R_ε is the relative efficiency between the signal and control modes obtained from simulated samples.

A set of external constraints is imposed on the signal model to ensure the stability of the amplitude fit in a similar fashion to Refs. [16, 38]: the CKM elements V_{tb} and V_{ts}^* are constrained to the values obtained from the SM fit of the Unitarity triangle [62]; the local FFs for the $B^0 \rightarrow K^{*0}$ transition are constrained to a combination [16, 32] of light-cone sum rules [25, 26] and lattice QCD [31] results; while for the S-wave amplitudes the local FFs are assumed to have the same q^2 dependence as in $B^+ \rightarrow K^+$ transitions and are constrained to the results of Ref. [29] but have their uncertainties inflated by a factor of three to account for the different meson species. An alternative choice of fixing the S-wave local FFs to the values from Ref. [63] is considered as a source of

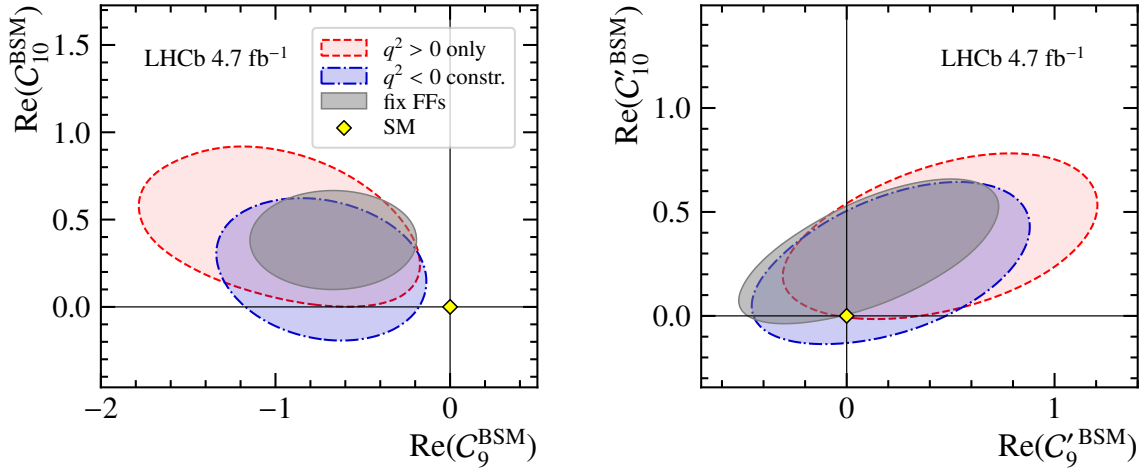


Figure 2: Two-dimensional profile-likelihood contours of the (left) $C_9^{\text{BSM}}-C_{10}^{\text{BSM}}$ and (right) $C_9'^{\text{BSM}}-C_{10}'^{\text{BSM}}$ pairs of Wilson coefficients at 68% confidence level with (blue) and without (red) SM constraints at $q^2 < 0$. The fit is also repeated considering local FFs to be fixed to their SM predictions (grey) [16, 25, 31].

systematic uncertainty. The magnitudes and phase differences of the resonant amplitudes for the $B^0 \rightarrow \psi_n K^{*0}$ decays are instrumental to constrain the values of \mathcal{H}_λ at the J/ψ and $\psi(2S)$ resonance poles. These are taken from measurements by both LHCb and B -factory experiments [61, 64–67]. Finally, the SM predictions for the real and imaginary parts of the ratio $\mathcal{H}_\lambda/\mathcal{F}_\lambda$ in the negative- q^2 region are taken from Refs. [16, 36] and are used as constraints in the fit.

Systematic uncertainties are studied using pseudoexperiments in which one or more parameters are varied and the values of interest are determined with and without this variation. The difference between the two sets of results is then taken as the associated systematic uncertainty. The total systematic uncertainty varies between 15 and 35% of the statistical uncertainty, depending on the considered Wilson coefficient. The dominant sources of systematic uncertainties are associated with the external branching fraction measurements entering in Eq. 3, where all the external inputs are varied within their uncertainties. The uncertainty on R_ϵ originates from the finite size of the simulated samples and from the model dependence of the simulation. The uncertainty on $f^{J/\psi K\pi}$ is determined from pseudoexperiments generated from the amplitude model of Ref. [61]. The systematic uncertainty due to ignoring non-local effects in the scalar amplitudes is assessed by generating pseudoexperiments where non-local FFs are assumed to be of the same order of those observed in the longitudinal P-wave amplitude. All other considered sources of systematic uncertainty are negligible.

The results of the fit to the data are shown in Fig. 2 (blue contours) as two-dimensional profile-likelihood projections for $C_9^{(\prime)\text{BSM}}$ and $C_{10}^{(\prime)\text{BSM}}$, where the superscript BSM indicates a difference with respect to the SM predictions. When allowing for non-local hadronic effects, the fit results still yield a C_9 value that is somewhat different from the SM prediction, however, the global significance of the differences in the Wilson coefficients is equivalent to 1.4 standard deviations (σ), considering both statistical and systematic uncertainties. In order to evaluate the compatibility of each Wilson coefficient with the

SM, one-dimensional profile likelihood scans are performed on the individual coefficients. The largest deviation is associated to a shift in \mathcal{C}_9 of -0.7 with a significance of 1.8σ . These results show a good qualitative agreement with global analyses of $b \rightarrow s\mu^+\mu^-$ transitions [16–19]. In comparison with the existing literature, the present analysis relies on the unbinned use of the experimental data, a z -expansion for the treatment of non-local contribution (as in Ref. [16]) and focus on only $B^0 \rightarrow K^{*0}\mu^+\mu^-$ data, while global analyses typically include data on other $b \rightarrow s\mu^+\mu^-$ processes.

The impact of long-distance contributions on the determination of the genuine short-distance effects can be better investigated by repeating the amplitude fit using alternative theory assumptions, as overlaid in Fig. 2. As a first test, the theory constraints at negative q^2 are removed from the fit. In this case, a second-order polynomial is sufficient to accommodate the non-local FF contributions and a point within the charmonium resonance region is used as a reference for the expansion. A similar compatibility to the SM is observed but with a larger statistical uncertainty (red contours). Another interesting behaviour is observed in the role of the local FFs in the determination of the non-local effects. Since the largest uncertainty on the theory prediction of \mathcal{H}_λ at negative q^2 is due to the local FF uncertainties [16, 36], there is intrinsically a strong correlation in the fit between the local and non-local parameters. As a result, removing the theory constraints at $q^2 < 0$ has an effect on the determination of the local FFs from the fit and, in turn, on all the Wilson coefficients. An overall shift in all the coefficients is observed between the two fit results. This behaviour is further studied by repeating the default fit with fixed local FF values (gray contours in Fig. 2). This artificial configuration, which assumes perfect knowledge of $\mathcal{F}_\lambda^{(T)}$, illustrates how the uncertainties associated to the local FFs dominate and prevent a clean extraction of \mathcal{C}_9 and \mathcal{C}_{10} .

Figure 3 (top) reports the determination of the angular observable P'_5 obtained from the full amplitude fit compared to the result of the previous binned angular analysis [10] and different sets of SM predictions [16, 25, 31, 33, 68]. A good consistency is found between the results of the binned and unbinned analyses. Figure 3 (centre) illustrates the contribution due to non-local hadronic effects to the P'_5 observable obtained in this analysis. This contribution is isolated by varying the non-local parameters within their uncertainties and subtracting the resulting value of the observable by the same quantity re-evaluated with the non-local parameters fixed to zero. Non-local effects are found to contribute with a small positive shift to the P'_5 observable in a direction that reduces the discrepancy between the SM and the data. The constraints imposed by the $q^2 < 0$ predictions significantly reduce the uncertainty on the non-local effects. In general, the impact of non-local contributions to the different angular observables is found to be consistent whether $q^2 < 0$ constraints are included or not in the fit. The only exception is the S_7 observable in Fig. 3 (bottom). Since a non-zero value of S_7 can only result from a strong phase difference between amplitudes, the observed trend indicates potentially large phase differences in data that can not be accounted for if the theory constraints at $q^2 < 0$ are applied. For completeness, the impact of the non-local effects on all the other angular observables is given in the Supplemental Material [69].

In summary, using pp collision data collected with the LHCb experiment between 2011 and 2016, a direct experimental determination of the short-distance contributions in the $B^0 \rightarrow K^{*0}\mu^+\mu^-$ decay is obtained for the first time, together with the most accurate characterisation to date of the impact of long-distance effects on the decay process. The results are consistent with the pattern of modifications to the Wilson coefficients

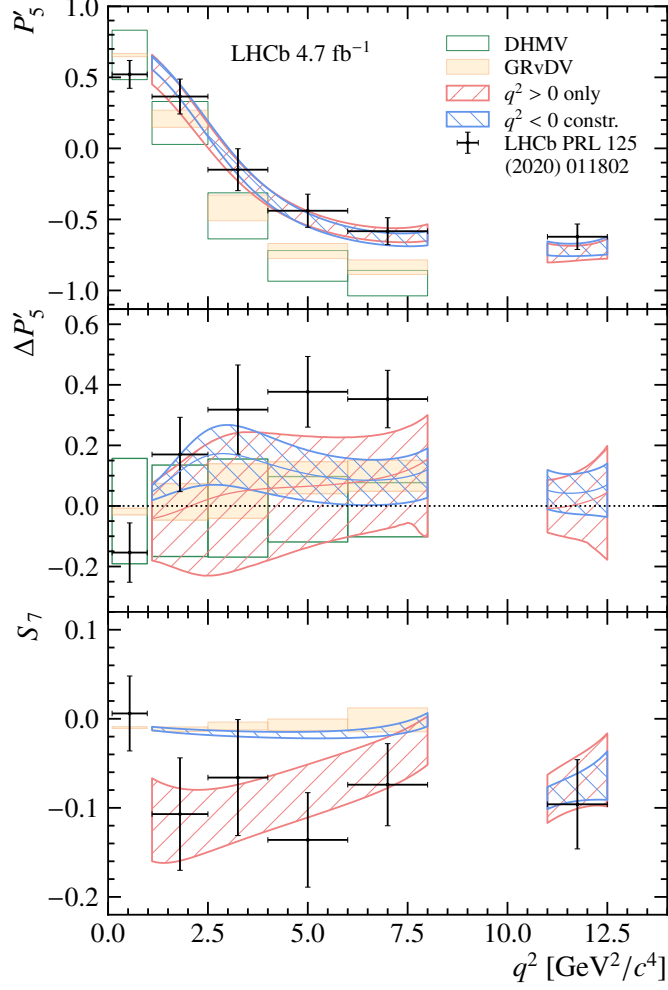


Figure 3: Determination of the (top) P'_5 and (bottom) S_7 angular observables obtained from the amplitude fit. Results are shown for fits with (blue) and without (red) constraints from $q^2 < 0$, at 68% confidence level. The LHCb binned angular analysis [10] (black dots) and SM predictions from DHMV [33,68] (green) and GRvDV [16,25,31] (yellow) are overlaid for reference. The center panel shows the non-local contributions to P'_5 determined from the amplitude fit. Here the difference between the LHCb binned angular analysis [10] and SM central value from DHMV is overlaid for reference (black dots), together with the uncertainty on the DHMV SM prediction (green) and difference between the SM predictions from GRvDV and DHMV (yellow). Theoretical predictions are shown only for $q^2 < 8 \text{ GeV}^2/c^4$.

suggested by global analyses of $b \rightarrow s\mu^+\mu^-$ processes, but the explicit inclusion of non-local contributions in the signal amplitude model is found to reduce the previously observed tension in the $B^0 \rightarrow K^{*0}\mu^+\mu^-$ decay to a level below two standard deviations.

Acknowledgements

We are very grateful to Nico Gubernari, MÉRil Reboud, Danny van Dyk, and Javier Virto for the many helpful discussions. We express our gratitude to our colleagues in

the CERN accelerator departments for the excellent performance of the LHC. We thank the technical and administrative staff at the LHCb institutes. We acknowledge support from CERN and from the national agencies: CAPES, CNPq, FAPERJ and FINEP (Brazil); MOST and NSFC (China); CNRS/IN2P3 (France); BMBF, DFG and MPG (Germany); INFN (Italy); NWO (Netherlands); MNiSW and NCN (Poland); MCID/IFA (Romania); MICINN (Spain); SNSF and SER (Switzerland); NASU (Ukraine); STFC (United Kingdom); DOE NP and NSF (USA). We acknowledge the computing resources that are provided by CERN, IN2P3 (France), KIT and DESY (Germany), INFN (Italy), SURF (Netherlands), PIC (Spain), GridPP (United Kingdom), CSCS (Switzerland), IFIN-HH (Romania), CBPF (Brazil), and Polish WLCG (Poland). We are indebted to the communities behind the multiple open-source software packages on which we depend. Individual groups or members have received support from ARC and ARDC (Australia); Key Research Program of Frontier Sciences of CAS, CAS PIFI, CAS CCEPP, Fundamental Research Funds for the Central Universities, and Sci. & Tech. Program of Guangzhou (China); Minciencias (Colombia); EPLANET, Marie Skłodowska-Curie Actions, ERC and NextGenerationEU (European Union); A*MIDEX, ANR, IPhU and Labex P2IO, and Région Auvergne-Rhône-Alpes (France); AvH Foundation (Germany); ICSC (Italy); GVA, XuntaGal, GENCAT, Inditex, InTalent and Prog. Atracción Talento, CM (Spain); SRC (Sweden); the Leverhulme Trust, the Royal Society and UKRI (United Kingdom).

Supplemental material

Figures 4 and 5 show the impact of non-local hadronic contributions to the angular observables in the P- and S-basis, respectively.

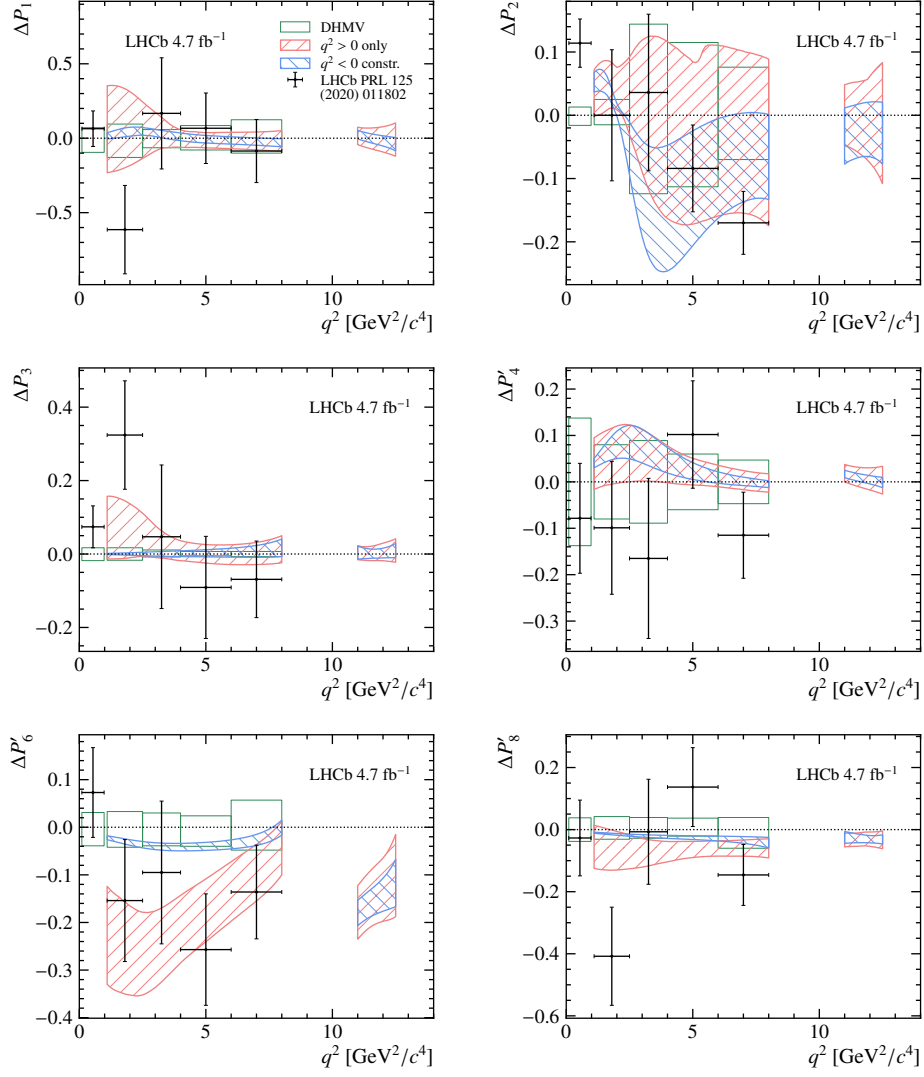
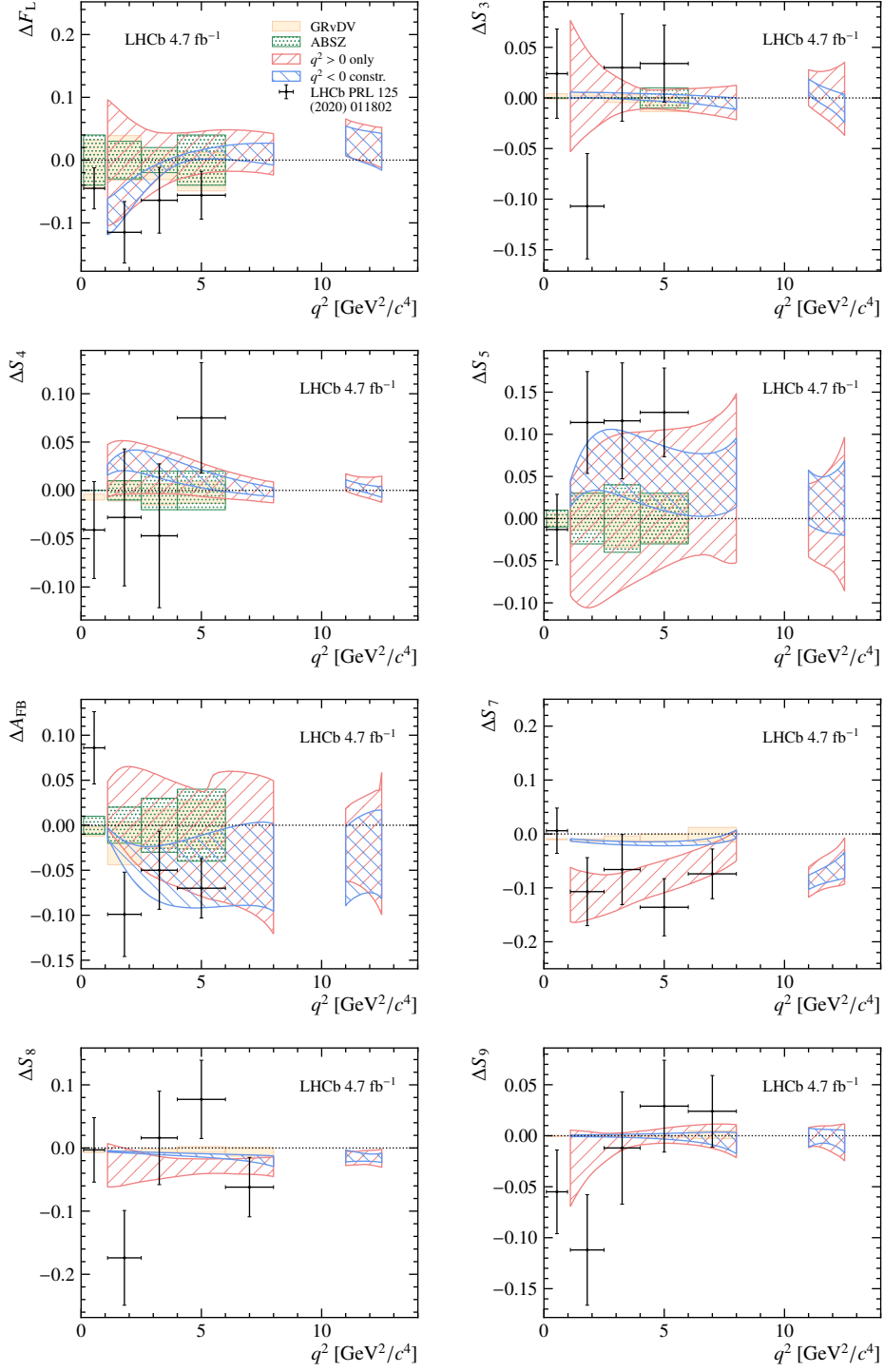


Figure 4: Non-local contributions to the angular observables (P-basis) obtained from data fits with (blue) and without (red) constraints from $q^2 < 0$. The shaded regions are shown at 68% confidence level. When available, the difference between the LHCb binned angular analysis [10] and SM central-value from Refs. [33, 68] is overlaid for reference (black dots), together with the uncertainty on the SM prediction (green).



References





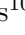
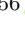


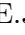
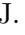

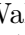




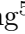






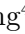




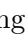
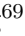













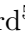
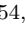









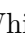

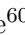


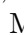
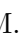

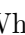
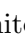







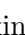

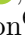
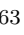






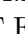


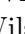

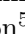






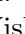
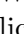

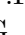

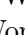

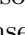
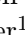

- [1] LHCb collaboration, R. Aaij *et al.*, *Differential branching fractions and isospin asymmetries of $B \rightarrow K^{(*)}\mu^+\mu^-$ decays*, JHEP **06** (2014) 133, arXiv:1403.8044.
- [2] LHCb collaboration, R. Aaij *et al.*, *Differential branching fraction and angular analysis of the decay $B_s^0 \rightarrow \phi\mu^+\mu^-$* , JHEP **07** (2013) 084, arXiv:1305.2168.
- [3] LHCb collaboration, R. Aaij *et al.*, *Differential branching fraction and angular analysis of $\Lambda_b^0 \rightarrow \Lambda\mu^+\mu^-$ decays*, JHEP **06** (2015) 115, Erratum *ibid.* **09** (2018) 145, arXiv:1503.07138.
- [4] LHCb collaboration, R. Aaij *et al.*, *Measurement of the $\Lambda_b^0 \rightarrow \Lambda(1520)\mu^+\mu^-$ differential branching fraction*, Phys. Rev. Lett. **131** (2023) 151801, arXiv:2302.08262.
- [5] LHCb collaboration, R. Aaij *et al.*, *Angular analysis of the $B^+ \rightarrow K^{*+}\mu^+\mu^-$ decay*, Phys. Rev. Lett. **126** (2021) 161802, arXiv:2012.13241.
- [6] LHCb collaboration, R. Aaij *et al.*, *Measurements of the S-wave fraction in $B^0 \rightarrow K^+\pi^-\mu^+\mu^-$ decays and the $B^0 \rightarrow K^*(892)^0\mu^+\mu^-$ differential branching fraction*, JHEP **11** (2016) 047, Erratum *ibid.* **04** (2017) 142, arXiv:1606.04731.
- [7] LHCb collaboration, R. Aaij *et al.*, *Differential branching fraction and angular analysis of the decay $B^0 \rightarrow K^{*0}\mu^+\mu^-$* , JHEP **08** (2013) 131, arXiv:1304.6325.
- [8] LHCb collaboration, R. Aaij *et al.*, *Measurement of form-factor-independent observables in the decay $B^0 \rightarrow K^{*0}\mu^+\mu^-$* , Phys. Rev. Lett. **111** (2013) 191801, arXiv:1308.1707.
- [9] LHCb collaboration, R. Aaij *et al.*, *Angular analysis of the $B^0 \rightarrow K^{*0}\mu^+\mu^-$ decay using 3 fb^{-1} of integrated luminosity*, JHEP **02** (2016) 104, arXiv:1512.04442.
- [10] LHCb collaboration, R. Aaij *et al.*, *Measurement of CP-averaged observables in the $B^0 \rightarrow K^{*0}\mu^+\mu^-$ decay*, Phys. Rev. Lett. **125** (2020) 011802, arXiv:2003.04831.
- [11] Belle collaboration, S. Wehle *et al.*, *Lepton-flavor-dependent angular analysis of $B \rightarrow K^*\ell^+\ell^-$* , Phys. Rev. Lett. **118** (2017) 111801, arXiv:1612.05014.
- [12] ATLAS collaboration, M. Aaboud *et al.*, *Angular analysis of $B_d^0 \rightarrow K^*\mu^+\mu^-$ decays in pp collisions at $\sqrt{s} = 8\text{ TeV}$ with the ATLAS detector*, JHEP **10** (2018) 047, arXiv:1805.04000.
- [13] CMS collaboration, A. M. Sirunyan *et al.*, *Measurement of angular parameters from the decay $B^0 \rightarrow K^{*0}\mu^+\mu^-$ in proton-proton collisions at $\sqrt{s} = 8\text{ TeV}$* , Phys. Lett. **B781** (2018) 517, arXiv:1710.02846.
- [14] S. Descotes-Genon, L. Hofer, J. Matias, and J. Virto, *Global analysis of $b \rightarrow s\ell\ell$ anomalies*, JHEP **06** (2016) 092, arXiv:1510.04239.
- [15] G. Buchalla, A. J. Buras, and M. E. Lautenbacher, *Weak decays beyond leading logarithms*, Rev. Mod. Phys. **68** (1996) 1125, arXiv:hep-ph/9512380.

- [16] N. Gubernari, M. Reboud, D. van Dyk, and J. Virto, *Improved theory predictions and global analysis of exclusive $b \rightarrow s\mu^+\mu^-$ processes*, JHEP **09** (2022) 133, [arXiv:2206.03797](#).
- [17] A. Greljo, J. Salko, A. Smolkovič, and P. Stangl, *Rare b decays meet high-mass Drell-Yan*, JHEP **05** (2023) 087, [arXiv:2212.10497](#).
- [18] M. Algueró *et al.*, *To $(b)e$ or not to $(b)e$: no electrons at LHCb*, Eur. Phys. J. **C83** (2023) 648, [arXiv:2304.07330](#).
- [19] M. Ciuchini *et al.*, *Constraints on lepton universality violation from rare B decays*, Phys. Rev. **D107** (2023) 055036, [arXiv:2212.10516](#).
- [20] S. Jäger and J. Martin Camalich, *On $B \rightarrow V\ell\ell$ at small dilepton invariant mass, power corrections, and new physics*, JHEP **05** (2013) 043, [arXiv:1212.2263](#).
- [21] S. Jäger and J. Martin Camalich, *Reassessing the discovery potential of the $B \rightarrow K^*\ell^+\ell^-$ decays in the large-recoil region: SM challenges and BSM opportunities*, Phys. Rev. **D93** (2016) 014028, [arXiv:1412.3183](#).
- [22] A. Khodjamirian and A. V. Rusov, *$B_s \rightarrow K\ell\nu_\ell$ and $B_{(s)} \rightarrow \pi(K)\ell^+\ell^-$ decays at large recoil and CKM matrix elements*, JHEP **08** (2017) 112, [arXiv:1703.04765](#).
- [23] A. Bharucha, D. M. Straub, and R. Zwicky, *$B \rightarrow V\ell^+\ell^-$ in the Standard Model from light-cone sum rules*, JHEP **08** (2016) 098, [arXiv:1503.05534](#).
- [24] A. Agadjanov, V. Bernard, U.-G. Meißner, and A. Rusetsky, *The $B \rightarrow K^*$ form factors on the lattice*, Nucl. Phys. **B910** (2016) 387, [arXiv:1605.03386](#).
- [25] N. Gubernari, A. Kokulu, and D. van Dyk, *$B \rightarrow P$ and $B \rightarrow V$ form factors from B -Meson light-cone sum rules beyond leading twist*, JHEP **01** (2019) 150, [arXiv:1811.00983](#).
- [26] S. Descotes-Genon, A. Khodjamirian, and J. Virto, *Light-cone sum rules for $B \rightarrow K\pi$ form factors and applications to rare decays*, JHEP **12** (2019) 083, [arXiv:1908.02267](#).
- [27] J. Gao *et al.*, *Precision calculations of $B \rightarrow V$ form factors from soft-collinear effective theory sum rules on the light-cone*, Phys. Rev. **D101** (2020) 074035, [arXiv:1907.11092](#).
- [28] HPQCD collaboration, C. Bouchard *et al.*, *Rare decay $B \rightarrow K\ell^+\ell^-$ form factors from lattice QCD*, Phys. Rev. **D88** (2013) 054509, [arXiv:1306.2384](#), [Erratum: Phys.Rev.D 88, 079901 (2013)].
- [29] J. A. Bailey *et al.*, *$B \rightarrow K\ell^+\ell^-$ decay form factors from three-flavor lattice QCD*, Phys. Rev. **D93** (2016) 025026, [arXiv:1509.06235](#).
- [30] R. R. Horgan, Z. Liu, S. Meinel, and M. Wingate, *Lattice QCD calculation of form factors describing the rare decays $B \rightarrow K^*\ell^+\ell^-$ and $B_s \rightarrow \phi\ell^+\ell^-$* , Phys. Rev. **D89** (2014) 094501, [arXiv:1310.3722](#).

- [31] R. R. Horgan, Z. Liu, S. Meinel, and M. Wingate, *Rare B decays using lattice QCD form factors*, PoS **LATTICE2014** (2015) 372, [arXiv:1501.00367](#).
- [32] N. Gubernari, M. Reboud, D. van Dyk, and J. Virto, *Dispersive analysis of $B \rightarrow K^{(*)}$ and $B_s \rightarrow \phi$ form factors*, [arXiv:2305.06301](#).
- [33] A. Khodjamirian, T. Mannel, A. A. Pivovarov, and Y.-M. Wang, *Charm-loop effect in $B \rightarrow K^{(*)}\ell^+\ell^-$ and $B \rightarrow K^*\gamma$* , JHEP **09** (2010) 089, [arXiv:1006.4945](#).
- [34] A. Khodjamirian, T. Mannel, and Y. M. Wang, *$B \rightarrow K\ell^+\ell^-$ decay at large hadronic recoil*, JHEP **02** (2013) 010, [arXiv:1211.0234](#).
- [35] S. Descotes-Genon, A. Khodjamirian, J. Virto, and K. K. Vos, *Light-cone sum rules for S-wave $B \rightarrow K\pi$ form factors*, JHEP **06** (2023) 034, [arXiv:2304.02973](#).
- [36] N. Gubernari, D. van Dyk, and J. Virto, *Non-local matrix elements in $B_{(s)} \rightarrow \{K^{(*)}, \phi\}\ell^+\ell^-$* , JHEP **02** (2021) 088, [arXiv:2011.09813](#).
- [37] C. Bobeth, M. Chrzaszcz, D. van Dyk, and J. Virto, *Long-distance effects in $B \rightarrow K^*\ell\ell$ from analyticity*, Eur. Phys. J. **C78** (2018) 451, [arXiv:1707.07305](#).
- [38] M. Chrzaszcz *et al.*, *Prospects for disentangling long- and short-distance effects in the decays $B \rightarrow K^*\mu^+\mu^-$* , JHEP **10** (2019) 236, [arXiv:1805.06378](#).
- [39] T. Hurth, C. Langenbruch, and F. Mahmoudi, *Direct determination of Wilson coefficients using $B^0 \rightarrow K^{*0}\mu^+\mu^-$ decays*, JHEP **11** (2017) 176, [arXiv:1708.04474](#).
- [40] LHCb collaboration, R. Aaij *et al.*, *Determination of short- and long-distance contributions in $B^0 \rightarrow K^{*0}\mu^+\mu^-$ decays*, Phys. Rev. **D109** (2024) 052009, [arXiv:2312.09102](#).
- [41] W. Altmannshofer *et al.*, *Symmetries and asymmetries of $B \rightarrow K^*\mu^+\mu^-$ decays in the Standard Model and beyond*, JHEP **01** (2009) 019, [arXiv:0811.1214](#).
- [42] F. Kruger and J. Matias, *Probing new physics via the transverse amplitudes of $B^0 \rightarrow K^{*0}(\rightarrow K^-\pi^+)\ell^+\ell^-$ at large recoil*, Phys. Rev. **D71** (2005) 094009, [arXiv:hep-ph/0502060](#).
- [43] Particle Data Group, R. L. Workman *et al.*, *Review of particle physics*, Prog. Theor. Exp. Phys. **2022** (2022) 083C01.
- [44] C. Bobeth, M. Misiak, and J. Urban, *Photonic penguins at two loops and m_t dependence of $BR[B \rightarrow X_s\ell^+\ell^-]$* , Nucl. Phys. **B574** (2000) 291, [arXiv:hep-ph/9910220](#).
- [45] M. Gorbahn and U. Haisch, *Effective Hamiltonian for non-leptonic $|\Delta F| = 1$ decays at NNLO in QCD*, Nucl. Phys. **B713** (2005) 291, [arXiv:hep-ph/0411071](#).
- [46] D. Becirevic and A. Tayduganov, *Impact of $B \rightarrow K_0^*\ell^+\ell^-$ on the New Physics search in $B \rightarrow K^*\ell^+\ell^-$ decay*, Nucl. Phys. **B868** (2013) 368, [arXiv:1207.4004](#).
- [47] C.-D. Lu and W. Wang, *Analysis of $B \rightarrow K_J^*(\rightarrow K\pi)\mu^+\mu^-$ in the higher kaon resonance region*, Phys. Rev. **D85** (2012) 034014, [arXiv:1111.1513](#).

- [48] LHCb collaboration, A. A. Alves Jr. *et al.*, *The LHCb detector at the LHC*, JINST **3** (2008) S08005.
- [49] LHCb collaboration, R. Aaij *et al.*, *LHCb detector performance*, Int. J. Mod. Phys. **A30** (2015) 1530022, [arXiv:1412.6352](#).
- [50] T. Sjöstrand, S. Mrenna, and P. Skands, *A brief introduction to PYTHIA 8.1*, Comput. Phys. Commun. **178** (2008) 852, [arXiv:0710.3820](#).
- [51] D. J. Lange, *The EvtGen particle decay simulation package*, Nucl. Instrum. Meth. **A462** (2001) 152.
- [52] Geant4 collaboration, J. Allison *et al.*, *Geant4 developments and applications*, IEEE Trans. Nucl. Sci. **53** (2006) 270.
- [53] Geant4 collaboration, S. Agostinelli *et al.*, *Geant4: A simulation toolkit*, Nucl. Instrum. Meth. **A506** (2003) 250.
- [54] M. Abadi *et al.*, *TensorFlow: Large-scale machine learning on heterogeneous systems*, [arXiv:1603.04467](#), software available from tensorflow.org.
- [55] F. James and M. Roos, *Minuit: A system for function minimization and analysis of the parameter errors and correlations*, Comput. Phys. Commun. **10** (1975) 343.
- [56] R. Brun and F. Rademakers, *ROOT: An object oriented data analysis framework*, Nucl. Instrum. Meth. **A389** (1997) 81.
- [57] A. Paul and D. M. Straub, *Constraints on new physics from radiative B decays*, JHEP **04** (2017) 027, [arXiv:1608.02556](#).
- [58] H. Akaike, *A new look at the statistical model identification*, IEEE Transactions on Automatic Control **19** (1974) 716.
- [59] T. Skwarnicki, *A study of the radiative cascade transitions between the Upsilon-prime and Upsilon resonances*, PhD thesis, Institute of Nuclear Physics, Krakow, 1986, DESY-F31-86-02.
- [60] D. Aston *et al.*, *A study of $K^- \pi^+$ scattering in the reaction $K^- p \rightarrow K^- \pi^+ n$ at 11 GeV/c*, Nucl. Phys. **B296** (1988) 493.
- [61] Belle collaboration, K. Chilikin *et al.*, *Observation of a new charged charmonium like state in $\bar{B}^0 \rightarrow J/\psi K^- \pi^+$ decays*, Phys. Rev. **D90** (2014) 112009, [arXiv:1408.6457](#).
- [62] CKMfitter Group, J. Charles *et al.*, *CP violation and the CKM matrix: Assessing the impact of the asymmetric B factories*, Eur. Phys. J. **C41** (2005) 1, [arXiv:hep-ph/0406184](#), Updated results from summer 2019 (post EPS 2019 conference).
- [63] M. Döring, U.-G. Meißner, and W. Wang, *Chiral dynamics and S-wave contributions in semileptonic B decays*, JHEP **10** (2013) 011, [arXiv:1307.0947](#).

- [64] BaBar collaboration, B. Aubert *et al.*, *Measurement of decay amplitudes of $B \rightarrow J/\psi K^*$, $\psi(2S)K^*$, and $\chi_{c1}K^*$ with an angular analysis*, Phys. Rev. **D76** (2007) 031102, [arXiv:0704.0522](#).
- [65] Belle collaboration, K. Chilikin *et al.*, *Experimental constraints on the spin and parity of the $Z(4430)^+$* , Phys. Rev. **D88** (2013) 074026, [arXiv:1306.4894](#).
- [66] LHCb collaboration, R. Aaij *et al.*, *Measurement of the polarization amplitudes in $B^0 \rightarrow J/\psi K^*(892)^0$ decays*, Phys. Rev. **D88** (2013) 052002, [arXiv:1307.2782](#).
- [67] LHCb collaboration, R. Aaij *et al.*, *Measurement of relative branching fractions of B decays to $\psi(2S)$ and J/ψ mesons*, Eur. Phys. J. **C72** (2012) 2118, [arXiv:1205.0918](#).
- [68] S. Descotes-Genon, L. Hofer, J. Matias, and J. Virto, *On the impact of power corrections in the prediction of $B \rightarrow K^* \mu^+ \mu^-$ observables*, JHEP **12** (2014) 125, [arXiv:1407.8526](#).
- [69] See supplemental material for the impact of non-local hadronic effects on the angular observables other than P'_5 and S_7 .
- [70] W. Altmannshofer and D. M. Straub, *New physics in $b \rightarrow s$ transitions after LHC run 1*, Eur. Phys. J. **C75** (2015) 382, [arXiv:1411.3161](#).

D. vom Bruch¹² , V. Vorobyev⁴¹ , N. Voropaev⁴¹ , K. Vos⁷⁶ , G. Vouters¹⁰ , C. Vrahas⁵⁶ , J. Walsh³² , E.J. Walton¹ , G. Wan⁶ , C. Wang¹⁹ , G. Wang⁸ , J. Wang⁶ , J. Wang⁵ , J. Wang⁴ , J. Wang⁷¹ , M. Wang²⁷ , N. W. Wang⁷ , R. Wang⁵² , X. Wang⁶⁹ , X. W. Wang⁵⁹ , Y. Wang⁸ , Z. Wang¹³ , Z. Wang⁴ , Z. Wang⁷ , J.A. Ward^{54,1} , N.K. Watson⁵¹ , D. Websdale⁵⁹ , Y. Wei⁶ , B.D.C. Westhenry⁵² , D.J. White⁶⁰ , M. Whitehead⁵⁷ , A.R. Wiederhold⁵⁴ , D. Wiedner¹⁷ , G. Wilkinson⁶¹ , M.K. Wilkinson⁶³ , M. Williams⁶² , M.R.J. Williams⁵⁶ , R. Williams⁵³ , F.F. Wilson⁵⁵ , W. Wislicki³⁹ , M. Witek³⁸ , L. Witola¹⁹ , C.P. Wong⁶⁵ , G. Wormser¹³ , S.A. Wotton⁵³ , H. Wu⁶⁶ , J. Wu⁸ , Y. Wu⁶ , K. Wyllie⁴⁶ , S. Xian⁶⁹ , Z. Xiang⁵ , Y. Xie⁸ , A. Xu³² , J. Xu⁷ , L. Xu⁴ , L. Xu⁴ , M. Xu⁵⁴ , Z. Xu¹¹ , Z. Xu⁷ , Z. Xu⁵ , D. Yang⁴ , S. Yang⁷ , X. Yang⁶ , Y. Yang^{26,L} , Z. Yang⁶ , Z. Yang⁶⁴ , V. Yeroshenko¹³ , H. Yeung⁶⁰ , H. Yin⁸ , C. Y. Yu⁶ , J. Yu⁶⁸ , X. Yuan⁵ , E. Zaffaroni⁴⁷ , M. Zavertyaev¹⁸ , M. Zdybal³⁸ , M. Zeng⁴ , C. Zhang⁶ , D. Zhang⁸ , J. Zhang⁷ , L. Zhang⁴ , S. Zhang⁶⁸ , S. Zhang⁶ , Y. Zhang⁶ , Y. Zhang⁶¹ , Y. Z. Zhang⁴ , Y. Zhao¹⁹ , A. Zharkova⁴¹ , A. Zhelezov¹⁹ , X. Z. Zheng⁴ , Y. Zheng⁷ , T. Zhou⁶ , X. Zhou⁸ , Y. Zhou⁷ , V. Zhovkovska⁵⁴ , L. Z. Zhu⁷ , X. Zhu⁴ , X. Zhu⁸ , Z. Zhu⁷ , V. Zhukov^{16,41} , J. Zhuo⁴⁵ , Q. Zou^{5,7} , D. Zuliani³⁰ , G. Zunica⁶⁰ .

¹*School of Physics and Astronomy, Monash University, Melbourne, Australia*

²*Centro Brasileiro de Pesquisas Físicas (CBPF), Rio de Janeiro, Brazil*

³*Universidade Federal do Rio de Janeiro (UFRJ), Rio de Janeiro, Brazil*

⁴*Center for High Energy Physics, Tsinghua University, Beijing, China*

⁵*Institute Of High Energy Physics (IHEP), Beijing, China*

⁶*School of Physics State Key Laboratory of Nuclear Physics and Technology, Peking University, Beijing, China*

⁷*University of Chinese Academy of Sciences, Beijing, China*

⁸*Institute of Particle Physics, Central China Normal University, Wuhan, Hubei, China*

⁹*Consejo Nacional de Rectores (CONARE), San Jose, Costa Rica*

¹⁰*Université Savoie Mont Blanc, CNRS, IN2P3-LAPP, Annecy, France*

¹¹*Université Clermont Auvergne, CNRS/IN2P3, LPC, Clermont-Ferrand, France*

¹²*Aix Marseille Univ, CNRS/IN2P3, CPPM, Marseille, France*

¹³*Université Paris-Saclay, CNRS/IN2P3, IJCLab, Orsay, France*

¹⁴*Laboratoire Leprince-Ringuet, CNRS/IN2P3, Ecole Polytechnique, Institut Polytechnique de Paris, Palaiseau, France*

¹⁵*LPNHE, Sorbonne Université, Paris Diderot Sorbonne Paris Cité, CNRS/IN2P3, Paris, France*

¹⁶*I. Physikalisches Institut, RWTH Aachen University, Aachen, Germany*

¹⁷*Fakultät Physik, Technische Universität Dortmund, Dortmund, Germany*

¹⁸*Max-Planck-Institut für Kernphysik (MPIK), Heidelberg, Germany*

¹⁹*Physikalisches Institut, Ruprecht-Karls-Universität Heidelberg, Heidelberg, Germany*

²⁰*School of Physics, University College Dublin, Dublin, Ireland*

²¹*INFN Sezione di Bari, Bari, Italy*

²²*INFN Sezione di Bologna, Bologna, Italy*

²³*INFN Sezione di Ferrara, Ferrara, Italy*

²⁴*INFN Sezione di Firenze, Firenze, Italy*

²⁵*INFN Laboratori Nazionali di Frascati, Frascati, Italy*

²⁶*INFN Sezione di Genova, Genova, Italy*

²⁷*INFN Sezione di Milano, Milano, Italy*

²⁸*INFN Sezione di Milano-Bicocca, Milano, Italy*

²⁹*INFN Sezione di Cagliari, Monserrato, Italy*

³⁰*Università degli Studi di Padova, Università e INFN, Padova, Padova, Italy*

³¹*INFN Sezione di Perugia, Perugia, Italy*

³²*INFN Sezione di Pisa, Pisa, Italy*

³³*INFN Sezione di Roma La Sapienza, Roma, Italy*

- ³⁴ INFN Sezione di Roma Tor Vergata, Roma, Italy
- ³⁵ Nikhef National Institute for Subatomic Physics, Amsterdam, Netherlands
- ³⁶ Nikhef National Institute for Subatomic Physics and VU University Amsterdam, Amsterdam, Netherlands
- ³⁷ AGH - University of Science and Technology, Faculty of Physics and Applied Computer Science, Kraków, Poland
- ³⁸ Henryk Niewodniczanski Institute of Nuclear Physics Polish Academy of Sciences, Kraków, Poland
- ³⁹ National Center for Nuclear Research (NCBJ), Warsaw, Poland
- ⁴⁰ Horia Hulubei National Institute of Physics and Nuclear Engineering, Bucharest-Magurele, Romania
- ⁴¹ Affiliated with an institute covered by a cooperation agreement with CERN
- ⁴² DS4DS, La Salle, Universitat Ramon Llull, Barcelona, Spain
- ⁴³ ICCUB, Universitat de Barcelona, Barcelona, Spain
- ⁴⁴ Instituto Galego de Física de Altas Enerxías (IGFAE), Universidade de Santiago de Compostela, Santiago de Compostela, Spain
- ⁴⁵ Instituto de Física Corpuscular, Centro Mixto Universidad de Valencia - CSIC, Valencia, Spain
- ⁴⁶ European Organization for Nuclear Research (CERN), Geneva, Switzerland
- ⁴⁷ Institute of Physics, Ecole Polytechnique Fédérale de Lausanne (EPFL), Lausanne, Switzerland
- ⁴⁸ Physik-Institut, Universität Zürich, Zürich, Switzerland
- ⁴⁹ NSC Kharkiv Institute of Physics and Technology (NSC KIPT), Kharkiv, Ukraine
- ⁵⁰ Institute for Nuclear Research of the National Academy of Sciences (KINR), Kyiv, Ukraine
- ⁵¹ University of Birmingham, Birmingham, United Kingdom
- ⁵² H.H. Wills Physics Laboratory, University of Bristol, Bristol, United Kingdom
- ⁵³ Cavendish Laboratory, University of Cambridge, Cambridge, United Kingdom
- ⁵⁴ Department of Physics, University of Warwick, Coventry, United Kingdom
- ⁵⁵ STFC Rutherford Appleton Laboratory, Didcot, United Kingdom
- ⁵⁶ School of Physics and Astronomy, University of Edinburgh, Edinburgh, United Kingdom
- ⁵⁷ School of Physics and Astronomy, University of Glasgow, Glasgow, United Kingdom
- ⁵⁸ Oliver Lodge Laboratory, University of Liverpool, Liverpool, United Kingdom
- ⁵⁹ Imperial College London, London, United Kingdom
- ⁶⁰ Department of Physics and Astronomy, University of Manchester, Manchester, United Kingdom
- ⁶¹ Department of Physics, University of Oxford, Oxford, United Kingdom
- ⁶² Massachusetts Institute of Technology, Cambridge, MA, United States
- ⁶³ University of Cincinnati, Cincinnati, OH, United States
- ⁶⁴ University of Maryland, College Park, MD, United States
- ⁶⁵ Los Alamos National Laboratory (LANL), Los Alamos, NM, United States
- ⁶⁶ Syracuse University, Syracuse, NY, United States
- ⁶⁷ Pontifícia Universidade Católica do Rio de Janeiro (PUC-Rio), Rio de Janeiro, Brazil, associated to ³
- ⁶⁸ School of Physics and Electronics, Hunan University, Changsha City, China, associated to ⁸
- ⁶⁹ Guangdong Provincial Key Laboratory of Nuclear Science, Guangdong-Hong Kong Joint Laboratory of Quantum Matter, Institute of Quantum Matter, South China Normal University, Guangzhou, China, associated to ⁴
- ⁷⁰ Lanzhou University, Lanzhou, China, associated to ⁵
- ⁷¹ School of Physics and Technology, Wuhan University, Wuhan, China, associated to ⁴
- ⁷² Departamento de Física, Universidad Nacional de Colombia, Bogota, Colombia, associated to ¹⁵
- ⁷³ Universität Bonn - Helmholtz-Institut für Strahlen und Kernphysik, Bonn, Germany, associated to ¹⁹
- ⁷⁴ Eotvos Lorand University, Budapest, Hungary, associated to ⁴⁶
- ⁷⁵ Van Swinderen Institute, University of Groningen, Groningen, Netherlands, associated to ³⁵
- ⁷⁶ Universiteit Maastricht, Maastricht, Netherlands, associated to ³⁵
- ⁷⁷ Tadeusz Kosciuszko Cracow University of Technology, Cracow, Poland, associated to ³⁸
- ⁷⁸ Department of Physics and Astronomy, Uppsala University, Uppsala, Sweden, associated to ⁵⁷
- ⁷⁹ University of Michigan, Ann Arbor, MI, United States, associated to ⁶⁶
- ⁸⁰ Departement de Physique Nucleaire (SPhN), Gif-Sur-Yvette, France

^a Universidade de Brasília, Brasília, Brazil

^b Centro Federal de Educação Tecnológica Celso Suckow da Fonseca, Rio De Janeiro, Brazil

^c Hangzhou Institute for Advanced Study, UCAS, Hangzhou, China

^d LIP6, Sorbonne Université, Paris, France

- ^e *Excellence Cluster ORIGINS, Munich, Germany*
- ^f *Universidad Nacional Autónoma de Honduras, Tegucigalpa, Honduras*
- ^g *Università di Bari, Bari, Italy*
- ^h *Università di Bologna, Bologna, Italy*
- ⁱ *Università di Cagliari, Cagliari, Italy*
- ^j *Università di Ferrara, Ferrara, Italy*
- ^k *Università di Firenze, Firenze, Italy*
- ^l *Università di Genova, Genova, Italy*
- ^m *Università degli Studi di Milano, Milano, Italy*
- ⁿ *Università di Milano Bicocca, Milano, Italy*
- ^o *Università di Padova, Padova, Italy*
- ^p *Università di Perugia, Perugia, Italy*
- ^q *Scuola Normale Superiore, Pisa, Italy*
- ^r *Università di Pisa, Pisa, Italy*
- ^s *Università della Basilicata, Potenza, Italy*
- ^t *Università di Roma Tor Vergata, Roma, Italy*
- ^u *Università di Siena, Siena, Italy*
- ^v *Università di Urbino, Urbino, Italy*
- ^w *Universidad de Alcalá, Alcalá de Henares , Spain*
- ^x *Universidade da Coruña, Coruña, Spain*
- ^y *Department of Physics/Division of Particle Physics, Lund, Sweden*
- [†] *Deceased*